Implicitness and stability of time domain integral equation scattering analyses

S J Dodson, S P Walker[†], M J Bluck

Mechanical Engineering Department, Imperial College of Science Technology and Medicine

ABSTRACT. Time domain integral equation analysis of scattering problems has been inhibited by the instability generally observed. Usual treatments are explicit. We here describe an implicit approach, which allows timesteps to be selected to model the temporal variation of the field, rather than being constrained to small values by the need for the wave propagation during a timestep to be less than the smallest nodal spacing. For realistic bodies, this alone can result in computational cost savings by a significant factor. We present an investigation of the stability of the implicit approach, and show that it is much less prone to instability than the explicit. For realistic bodies, with rationally chosen timesteps, the implicit approach is for all practical purposes stable. This is so without recourse to the various temporal averaging schemes which have been proposed for stabilisation of the explicit form.

1. INTRODUCTION

Analysis of electromagnetic scattering via time domain techniques is increasingly employed[1]. For truly transient applications (as emp and emc can be) the advantages are obvious. Otherwise, broad band responses may be of interest, or even for a single frequency computational costs can actually scale less badly than those of frequency domain approaches[2]. The most widely used time domain technique is finite difference time domain, FDTD[3].

A discouragement from use of time domain integral equation methods has been that they are often found to be unstable. Almost all such studies reported[4-9], and all associated analysis of stability, have been for explicit formulations. These references include a body of work investigating this instability, with various essentially averaging procedures proposed to inhibit it; this we will discuss further below.

We have earlier described[10-12] an implicit formulation and noted that it is for all practical purposes stable, and similar observations have been made by Gravelle[13]. In this present paper we will investigate the stability of the implicit approach, and will identify a simple criterion via which the user can attain stability.

It is a curvilinear isoparametric approach, with the temporal variation similarly represented by quadratic shape functions. As noted, the approach is implicit; that is, the timestep Δt can be as large as is required to model adequately the temporal variation (and constrained ultimately by sampling theory), rather than be limited by the requirement that the distance the wave propagates in a timestep, $c\Delta t$, be less than the smallest nodal separation Δx.

This generalisation of the choice of timestep has two important practical consequences.

(i) On smooth regions of the body the discretisation will be determined by the wavelength (pulsewidth) of the field variation, but local mesh refinement is often needed to model geometrical features. An explicit formulation constrains the timestep to a value small enough to suit the smallest meshed spacing, with a corresponding multiple in computational costs. An implicit approach allows the timestep to be no smaller than is required to model the temporal variation of the field.

(ii) It provides stability, as we shall see below. From a large number of calculations of scattering from a variety of targets, selecting the timestep as will be discussed below, we have found stability problems in only a handful of cases, and this is then readily circumvented.

In the next section we will discuss the literature associated with stability of scattering calculations. In section 3 we develop the discretised form of the time domain integral equation. In section 4 we will consider its stability properties algebraically, and investigate them practically.

[†]London SW7 2BX, s.p.walker@ic.ac.uk

2. LITERATURE REVIEW

In 1985 Rynne[4] addressed the issue of stability of explicit time domain treatments of scattering problems. Exponentially growing errors were observed, changing sign at each timestep. It was concluded that their main source was in the numerical evaluation of the time derivative (of function f, at timestep k+1), and that careful evaluation of this term was required. The actual remedy proposed was in fact use of a generally less accurate time derivative approximation (namely $f'^{k+1} = \left(f^{k+1} - f^{k-1}\right)/2\Delta t$, rather than $f'^{k+1} = \left(f^{k+1} - f^{k}\right)/\Delta t$), on the grounds that it tended to cancel the oscillatory errors. The following year Rynne[5] proposed a more accurate time derivative approximation which also cancels errors. He also claims that the instabilities are related to the natural frequencies of the associated interior problem, and proposes spatial and temporal smoothing procedures to suppress them. The temporal version involves a retrospective averaging: $f^k = \left(f^{k+1} + 2f^k + f^{k-1}\right)/4$, which seems to suppress the instability with modest loss in accuracy.

Again for an explicit approach, in 1990 Smith[6] also suggests that the instabilities are associated with internal resonances, and discusses the matrix relationship $f^{k+1} = Mf^k$ between solutions at successive timesteps. This relationship is a special case of the more general implicit form, which we will return to below. He goes on to show that the retrospective averaging noted above has the effect of modifying the eigenvalues of the matrix M, and suggests that this will almost certainly stabilise the solution. In the examples quoted the retrospective averaging degrades the accuracy of the results by ~4% of their peak value. The process doubles the computational cost if employed at each timestep, but it was found sufficient to use it only occasionally, to eliminate instabilities as they began to become troublesome, and then to wait for their reappearance.

In 1991 Rao and Wilton[7] presented explicit time domain scattering computations, using essentially the simplest time derivative approximation noted above, and observed instabilities. In the following year Vechinski and Rao[8] proposed methods to stabilise the earlier work. They employ a temporal retrospective averaging, and this same averaging scheme has recently (1994) been employed[9] by the same authors to stabilise similar analyses of scattering from dielectric targets.

3. IMPLICIT FORMULATION

We will consider analysis of electromagnetic (MFIE) scattering from a perfect conductor embedded in dielectric, although we believe the observations are more general, and certainly from our own experience apply directly to scalar (acoustic) problems[14]. For any point $\mathbf{r}$ on the surface of the body, the field is given by an integral over the rest of the surface ($\mathbf{r}'$ and s') of the history of the field there. With $\mathbf{R} = \mathbf{r}' - \mathbf{r}$, with wave speed c, and time t and retarded time $t^* = t - R/c$, we have

$$2\pi\mathbf{H}(\mathbf{r},t) = 4\pi\mathbf{H}_{inc}(\mathbf{r},t) + \int_{\partial\Omega}\left(\mathbf{n}'\times\mathbf{H}(\mathbf{r}',t^*)\right)\times\frac{\hat{\mathbf{R}}}{R^2} + \left(\mathbf{n}'\times\frac{\partial\mathbf{H}}{\partial t}(\mathbf{r}',t^*)\right)\times\frac{\hat{\mathbf{R}}}{cR}\,ds' \tag{1}$$

More details of the numerical treatment are available elsewhere[10, 11, 14], but in essence the surface is divided into elements, over which the geometry is approximated using polynomial functions:

$$S_\alpha(\xi,\eta) \qquad \alpha = 1,..,9 \tag{2}$$

where ξ,η are the parameterised spatial co-ordinates. We will here use 9 noded quadrilaterals, but in principle a wide range may be employed. The geometry of each element is thus described by

$$\mathbf{r}^m(\xi,\eta) = \sum_{\alpha=1}^{9} S_\alpha(\xi,\eta)\mathbf{r}_{j(m,\alpha)} \tag{3}$$

where $j = j(m,\alpha)$ are the global node numbers of the local nodes on element m, and $\mathbf{r}_{j(m,\alpha)}$ is the position vector of each of these nodes.

The vector from the ith spatial node to some (ξ,η) co-ordinate location on the mth spatial element is then

$$\mathbf{R}(\mathbf{r}_i;\xi,\eta)\big|_m = \mathbf{r}_i - \sum_{\alpha=1}^{9} S_\alpha(\xi,\eta)\mathbf{r}_{j(m,\alpha)} \tag{4}$$

Explicitly indicating the dependence of t^* on R, and with $|\mathbf{J}(\xi,\eta)|$ the Jacobian, (1) can be written

$$2\pi\mathbf{H}(\mathbf{r},t) = 4\pi\mathbf{H}_{inc}(\mathbf{r},t)$$
$$+\sum_{m=1}^{M}\iint_{\xi,\eta}\left\{\sum_{\alpha=1}^{9}S_\alpha(\xi,\eta)\left(\mathbf{n}'\times\mathbf{H}(\xi,\eta;t^*(R,t))\right)\times\frac{\mathbf{R}}{R^3}\right\}|\mathbf{J}(\xi,\eta)|d\xi d\eta$$
$$+\sum_{m=1}^{M}\iint_{\xi,\eta}\left\{\sum_{\alpha=1}^{9}S_\alpha(\xi,\eta)\left(\mathbf{n}'\times\frac{\partial\mathbf{H}}{\partial t}(\xi,\eta;t^*(R,t))\right)\times\frac{\mathbf{R}}{cR^2}\right\}|\mathbf{J}(\xi,\eta)|d\xi d\eta \tag{5}$$

Using an isoparametric formulation, the spatial variation of the surface magnetic field over an element m may be written

$$\mathbf{H}(\xi,\eta;t)\big|_m = \sum_{\alpha=1}^{9}S_\alpha(\xi,\eta)\mathbf{H}_{j(m,\alpha)}(t) \tag{6}$$

We model the temporal variation using quadratic elements of length $2\Delta t$, with associated basis functions $T_\beta(\tau)$, with τ the intrinsic time. The temporal variation of the magnetic field over a temporal element l is

$$\mathbf{H}_{j(m,\alpha)}(\tau)\big|_l = \sum_{\beta=1}^{3}T_\beta(\tau)\mathbf{H}_{j(m,\alpha)}^{k(l,\beta)} \tag{7}$$

where $k = k(l,\beta)$ are the global timestep numbers of the local temporal nodes on temporal element l, and $\mathbf{H}_{j(m,\alpha)}^{k(l,\beta)}$ are the field values at the spatial nodes, at the three timesteps of the temporal element within which the time of interest falls.

We thus approximate the field at some intrinsic location ξ,η within spatial element m, at an intrinsic time τ within temporal element l, as

$$\mathbf{H}(\xi,\eta,\tau)\big|_{m,l} = \sum_{\alpha=1}^{9}\sum_{\beta=1}^{3}S_\alpha(\xi,\eta)T_\beta(\tau)\mathbf{H}_{j(m,\alpha)}^{k(l,\beta)} \tag{8}$$

Any particular location in (space, time) will lie in a single (spatial, temporal) element. Thus for a nine noded quadrilateral spatial element, and a three noded temporal element, the field at some location in it, at some time in it, is expressed as the weighted sum of the 27 (spatial and temporal) nodal values which surround it in the 'space-time' box.

We now evaluate the field for a particular timestep k+1, with $t = (k+1)\Delta t$. For the lossless dielectric of interest we require historical field values at retarded times. It is convenient to arrange that the present timestep, k+1, for which the field is being found, forms the final node of a temporal element. We then compute the number , l^*, of time elements ago that the element in which the relevant retarded time falls, via;

$$l^* = \text{int}\left\{\frac{R/c}{2\Delta t}\right\} \tag{9}$$

and identify the set of timestep numbers $k(l^*,\beta) = k - 2l^* - 2 + \beta$ associated with that element. The intrinsic time $\tau(R)$ within the element l^* corresponding to the retarded time is then found via

$$\tau(R) = \frac{(2l^*+1)\Delta t - R/c}{\Delta t} \tag{10}$$

We may then write equation (5), using (6) to (10), as

$$2\pi\mathbf{H}_i^{k+1} = 4\pi\mathbf{H}_{inc,i}^{k+1}$$
$$+\sum_{m=1}^{M}\iint_{\xi\eta}\sum_{\alpha=1}^{9}S_\alpha(\xi,\eta)\{W\}|\mathbf{J}(\xi,\eta)|d\xi d\eta$$
$$\{W\} = \sum_{\beta=1}^{3}\left(\frac{T_\beta(\tau(R))}{R^3} + \frac{\dot{T}_\beta(\tau(R))}{c\Delta t R^2}\right)\left[\left(\mathbf{n}'\times\mathbf{H}_{j(m,\alpha)}^{k(l^*,\beta)}\right)\times\mathbf{R}\right] \tag{11}$$

Integration over a single one of the M elements in the summation in (11), generating a contribution $\delta\mathbf{H}_m$ to the field, can be performed using Gaussian quadrature of order $NG \times NG$:

$$\delta\mathbf{H}_m = \sum_{p=1}^{NG}\sum_{q=1}^{NG}\sum_{\alpha=1}^{9}S_\alpha(\xi_p,\eta_q)\{W\}|\mathbf{J}(\xi_p,\eta_q)|w_p w_q \tag{12}$$

where the weights are w, and the dependence of R and n has been omitted for clarity. Part of the kernel of (12) is conveniently expressed by writing $(\mathbf{n}'\times\mathbf{H})\times\mathbf{R}$ as a $[A']\mathbf{H}$, with the matrix $[A']$ given by:

$$[A'] = \begin{bmatrix} n_2'R_2 + n_3'R_3 & -n_1'R_2 & -n_1'R_3 \\ -n_2'R_1 & n_1'R_1 + n_3'R_3 & -n_2'R_3 \\ -n_3'R_1 & -n_3'R_2 & n_1'R_1 + n_2'R_2 \end{bmatrix} \tag{13}$$

so that (12) becomes

$$\delta\mathbf{H}_m = \sum_{p=1}^{NG}\sum_{q=1}^{NG}\sum_{\alpha=1}^{9} S_\alpha(\xi_p,\eta_q) \sum_{\beta=1}^{3}\left(\frac{T_\beta(\tau(R))}{R^3}+\frac{\dot{T}_\beta(\tau(R))}{c\Delta t R^2}\right)[A']\mathbf{H}^{k(i^*,\beta)}_{j(m,\alpha)}\left|\mathbf{J}(\xi_p,\eta_q)\right| w_p w_q \tag{14}$$

Note that the retarded time associated with different Gaussian locations in a given spatial element may well fall in different temporal elements. Each such location would generate 3 sets of 9 coefficients. Since the temporal elements would be adjacent, the first and last sets of nine would generally be common to the adjacent temporal elements, resulting in 9 x 3, 9 x 5, 9 x 7, ...and so on possible distinct coefficients resulting from integration over a single element.

Evaluation of the quadrature summations thus yields a contribution to the field as a weighted sum of the nodal values of historical field. Special treatments[11, 15] are required for the singular and hypersingular integrands which arise when the field node i lies in the element m over which integration is being performed.

Thus far we have implicitly allowed the field $\mathbf{H}$ to have three (say) cartesian components, such that integrations of matrix $[A']$ would result in 3 by 3 matrices (for each node, and repeated for each temporal node). Application of the perfect conductor boundary conditions permits one of the three $\mathbf{H}$ components to be expressed as a linear combination of the other two, in turn reducing the results of the integrations to 2 by 2 (sub)matrices.

Writing these 2 by 2 submatrices as α, we can assemble all M of equations (14), and then write (11) as

$$2\pi\mathbf{H}_i^{k+1} = 4\pi\mathbf{H}_{inc,i}^{k+1} + \sum_{j=1}^{N}\sum_{w=0}^{W}\alpha_{i,j}^{w}\mathbf{H}_j^{k+1-w} \tag{15}$$

Here we have written the submatrices α as a complete three dimensional array; layers of size nodes by nodes, with as many layers as the W timesteps in a single transit. The submatrix $\alpha_{i,j}^{w}$ gives the influence of the field at node j at timestep k+1-w on the field at node i at timestep k+1.

Each layer is individually very sparse; recall integration over a single element results in coefficients relating to only a small number of adjacent temporal elements for each node, a consequence of the Dirac delta in the Green function in a lossless dielectric. In any one i,j location (field node, boundary node combination) there will be one group of adjacent non-zero layers, typically 3, or maybe 5 or 7 in number. All other entries will be zero.

Equation (15) expresses the field at a given location, at any particular timestep k+1, as a weighted sum of field values elsewhere on the surface at retarded times up to one transit time ago. Some of these historical values will be from less than Δt ago (those associated with w=0, or timestep k+1 itself) and others not. All field values at timestep k+1 and their associated weights are moved to the left hand side:

$$2\pi\mathbf{H}_i^{k+1} - \sum_{j=1}^{N}\alpha_{i,j}^{0}\mathbf{H}_j^{k+1} = 4\pi\mathbf{H}_{inc,i}^{k+1} + \sum_{j=1}^{N}\sum_{w=1}^{W}\alpha_{i,j}^{w}\mathbf{H}_j^{k+1-w} \tag{16}$$

where the lower limit on the temporal summation on the right hand side has consequently become 1.

When it is written as a single equation for the set of all N surface nodes i the coefficients on the left hand side of (16) form a matrix $[a]$, say (with the 2π term taken onto the diagonal of $[a]$). Matrix $[a]$ only has entries multiplying the field values presently being sought. It is sparse; on any one row it has entries only for nodes associated with quadrature locations falling within the $2c\Delta t$ radius sphere centred on the node in question; that is, for locations where the retarded time lies within the support of the temporal shape function associated with the present timestep.

The matrix formed by the coefficients on the right hand side of (16) has W layers, w=1 to W, (as opposed to the single w=0 layer of $[a]$) reflecting the fact that historical values from up to one transit time ago will influence the present field.

Everything on the right hand side of (16) is known, and can be multiplied out and added to the incident wave term to form a vector, $[c]$ say. At each timestep we thus generate the required set of new surface field values by solving the sparse matrix equation:

$$[a]\mathbf{H}^{k+1} = [c] \tag{17}$$

Implicitness / explicitness

Note that if we were to reduce the timestep we would recover an explicit formulation. The matrix $[a]$ on the left of (17) would become wholly diagonal, with all new field values able to be found independently of

each other by simple summation of historical values. It is the distance from the field node i to the nearest Gauss quadrature locations which is the determinant of the degree of implicitness. Quadrature locations lying within a sphere of radius $2c\Delta t$ of the field node will cause there to be a contribution at node i from the field about to be calculated at the neighbouring node. It is actually rather difficult to engineer an explicit treatment once even low order Gaussian quadrature is used for the integrations. For an edge node of a simple rectangular mesh of unit nodal spacing, with only 2 by 2 quadrature, influence from adjacent new field values occurs with a timestep of ~0.2. For 4 by 4, the order we normally employ, this falls to ~0.07 . Once this threshold is crossed, there are at least O(10), and in practical meshes many tens of non-zero entries on each line of $[a]$ on the left of (17). With similar (say quadratic) modelling of the spatial and temporal variation, the smallest timestep it is rational to select is about equal to one nodal spacing; about 14 times the timestep beyond which implicitness arises.

One consequence of implicitness is that a matrix equation (equation (17)) must be solved at each time step. For other than electrically small bodies matrix $[a]$ is sparse, with only a fraction of nodes having entries on each row of $[a]$. We normally solve $[a]$ at each timestep using an iterative method, such as the conjugate gradient or 'conjugate gradient squared' approaches. With such sparsity, and a very good initial guess available from the solution at the previous timestep, the cost of this is insignificant, and declines as a fraction of total cost as larger problems are addressed[16]. The dominant computational cost is the summations of (16), just as with an explicit approach.

4. INVESTIGATION OF STABILITY

4.1 Algebraic stability analysis

We now consider approaches to the analysis of stability of the above procedure. The most natural approach would be to obtain bounds on the behaviour of successive vectors $\mathbf{H}^k$ in (17), in terms of the properties of the associated matrices. However, as it stands, (17) does not provide a direct relationship between successive $\mathbf{H}$ vectors; the field at any one time is affected directly by all the previous field in the last transit time, via:

$$-\alpha^0\mathbf{H}^{k+1} = 4\pi\mathbf{H}_{inc}^{k+1} \qquad (18)$$
$$+\alpha^1\mathbf{H}^{k} + \alpha^2\mathbf{H}^{k-1} + \alpha^2\mathbf{H}^{k-2} \ldots\ldots + \alpha^W\mathbf{H}^{k+1-W}$$

where the bold unsubscripted α denotes the N by N matrix of submatrices.

Expressing recursively each $\mathbf{H}$ in terms of earlier $\mathbf{H}$ vectors, and for times after the incident wave has passed, it is possible to write down a relationship of the form

$$\mathbf{H}^{k+1} = \left[\Omega^{k+1}\right]\mathbf{H}^0 \qquad (19)$$

where the time dependent matrix Ω is a collection of powers of the matrices formed by the (submatrix) coefficients α. This is difficult and expensive to evaluate.

An alternative approach is to examine the relationship between successive sets of vectors of field values spanning one transit time. Forming a composite vector by of length (N x W) by listing together successive solution vectors, we can write a matrix equation relating successive such composite vectors (again, once the incident field has passed):

$$\begin{bmatrix} \alpha^0 & & & \\ & 1 & & \\ & & 1 & \\ & & & 1 \end{bmatrix} \begin{bmatrix} \mathbf{H}^{k+1} \\ \mathbf{H}^{k} \\ \mathbf{H}^{k-1} \\ \mathbf{H}^{k+1-W} \end{bmatrix} = \begin{bmatrix} \alpha^1 & \alpha^2 & \alpha^3 & \alpha^W \\ 1 & & & \\ & 1 & & \\ & & 1 & \end{bmatrix} \begin{bmatrix} \mathbf{H}^{k} \\ \mathbf{H}^{k-1} \\ \mathbf{H}^{k-2} \\ \mathbf{H}^{k-W} \end{bmatrix} \qquad (20)$$

where matrix coefficients are zero unless indicated. Recall that each individual coefficient of the two matrices above is itself an N by N matrix of 2 by 2 submatrices. Denoting the composite vector as $\mathbf{h}^k$, and the two matrices A and B, we can write the relationship between successive composite field vectors as

$$\mathbf{h}^{k+1} = \left[A^{-1}B\right]\mathbf{h}^k = M\mathbf{h}^k \qquad (21)$$

It is the properties of the matrix M:

$$M = \begin{bmatrix} \begin{bmatrix} (\alpha^0)^{-1} & & \\ & 1 & \\ & & 1 \\ & & & \ddots \\ & & & & 1 \end{bmatrix} \begin{bmatrix} \alpha^1 & \alpha^2 & \alpha^3 & & \alpha^W \\ 1 & & & & \\ & 1 & & & \\ & & & \ddots & \\ & & & & 1 \end{bmatrix} \end{bmatrix} =$$

$$\begin{bmatrix} (\alpha^0)^{-1}\alpha^1 & (\alpha^0)^{-1}\alpha^2 & (\alpha^0)^{-1}\alpha^3 & & (\alpha^0)^{-1}\alpha^W \\ 1 & & & & \\ & 1 & & & \\ & & & \ddots & \\ & & & & 1 \end{bmatrix} \tag{22}$$

and in particular the modulus of its largest eigenvalue, which will determine the long term stability of the system.

Although the details are rather different, for the special case of explicitness this reduces to the form discussed by Smith[6]. The left hand side matrix α^0 does not arise in that case, and stability then is determined by the properties of B, rather than the $A^{-1}B$ product of (21) here.

4.2 Numerical results

Unit radius sphere		Unit side cube		Almond 9.936 long	
98	0.39	26	0.5	594	0.54
258	0.26	98	0.25	1202	0.37
674	0.16	218	0.17		
		386	0.125		
		602	0.1		
		1178	0.07		

Table 1. Geometries and meshes (nodes and typical nodal spacing) used in example computations.

The general issue of the effectiveness of the present IETD approach, and comparison of its predictions with experiment, analytical results and other computations, and assessment of accuracy as a function of nodal separation and timestep, is reported elsewhere[11, 17, 18]. It has proven to be robust and effective, capable of predicting the scattering from large (eg 26 wavelengths, 41,000 node) bodies.

For convenience, relevant parameters for the various test cases employed are summarised in table 1. In all cases excitation was by a Gaussian pulse, of unit wavespeed, unit magnitude peak value, and with a width at half maximum of 3 for the spheres and almond[19], and 3.2 for the cubes.

4.2.1 Eigenvalues and Stability

Practical investigation of stability and associated eigenvalues is rather difficult. The matrix products $(\alpha^0)^{-1}\alpha^w$ are each dense, of size $4N$ by $4N$, and there are W of them in the upper part of M. For even the 98 node sphere, for example, M is of size ~2 000 by 2 000.

The field history on the 98 node sphere is shown in figure 1, for cases with timesteps of 0.17 and 0.2 transits. The latter is seen to be stable; the short horizontal portion of the response shown at t=200 continues indefinitely, whilst the other exhibits instability, albeit not till after about 70 transits.

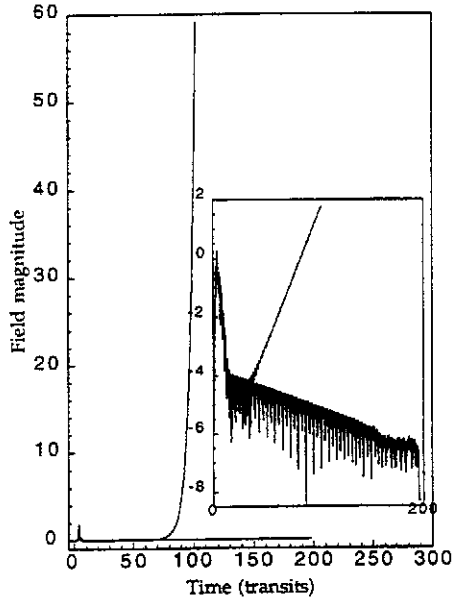

Figure 1 Field (log inset) versus time (in transits) on the 98 node sphere; timesteps of 0.17 transits (upper curve) and 0.2 transits.

Figure 2 shows the distribution of the eigenvalues of M for these two cases. For the indefinitely stable

timestep the maximum modulus is 0.987, whilst for the unstable one it is 1.052.

In figure 3 we show the variation of maximum eigenvalue modulus for a wide range of timesteps used for analysis of the 26 node cube. There is a clear general drift towards maximum modulus values below one as the timestep is increased. Additionally (not shown) the number of eigenvalues above one also declines as the timestep is increased. These cases are associated with stable long term responses. This behaviour is broadly consistent over both the sphere and cube meshes.

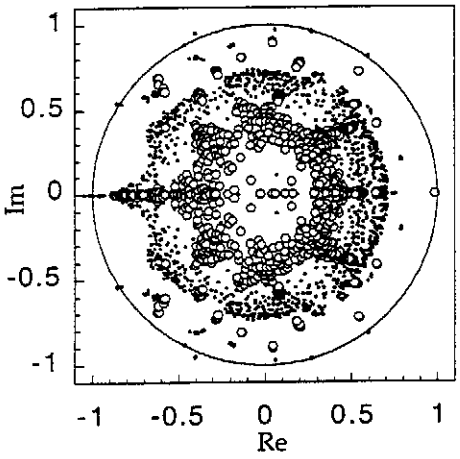

Figure 2 Eigenvalues of matrix M, for analysis of the 98 node sphere with timesteps of 0.17 transits (black) and 0.2 transits (white).

Note that this move into a region of lower eigenvalues is only available via the implicit treatment. Indeed, for the larger ~half of the timesteps employed, this (small) problem is wholly implicit; all nodes have associated quadrature locations lying within $c\Delta t$ of every other node.

4.2.2 Empirical investigations

It has been demonstrated above that it is the eigenvalues of M which determine stability. We have also shown a number of examples where increasing the timestep decreased the maximum eigenvalue, and stability followed. It remains to identify how to select modelling parameters to achieve this. For practical three dimensional, arbitrary geometries, it is no easier to identify parameters which will achieve eigenvalues of M below one than to identify directly parameters required to achieve stability, and it is on this which we will concentrate subsequently, by empirical investigation.

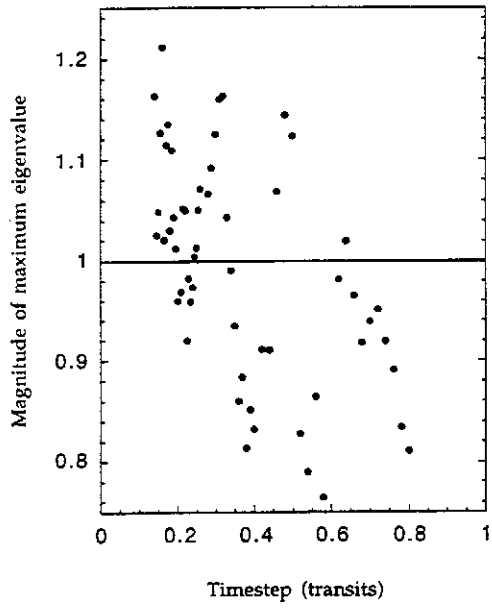

Figure 3 Maximum eigenvalue versus timestep for the 26 node cube

We will first consider what, numerically, constitutes total stability. For a propagation problem such as we are considering, with an incident wave, an unchanging field will occur only when the field is zero. Accordingly, we terminate the calculation when (once the incident wave has arrived)

$$\left\|\mathbf{H}^{k+1}-\mathbf{H}^{k}\right\|_2 \le 10^{-6} \qquad (23)$$

The calculation was continued beyond this point on a number of occasions, to test this. As expected, an endless series of identically zero (to numerical precision) vectors $\mathbf{H}$ is generated.There are two (coupled) aspects to instability; the time till the field begins its oscillatory exponential increase, and the rate of this increase.

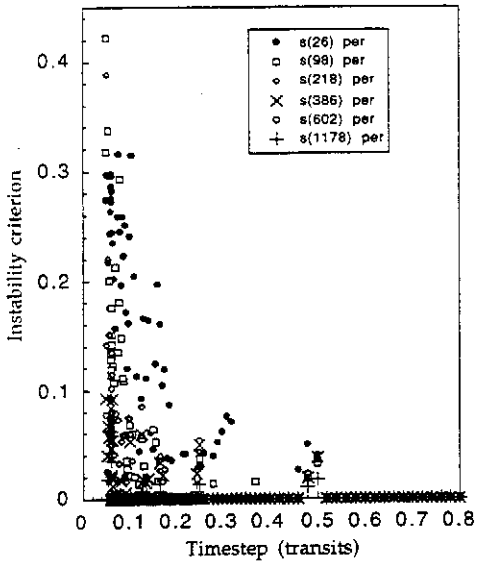

Figure 4. Instability criterion (the reciprocal of the number of pulse widths till the field re-attains the incident field magnitude) versus timestep in transit times, for various cube meshes.

We will adopt a measure of instability which incorporates both. We take as a criterion the reciprocal of the time required for the field to reach again the magnitude of the incident field. This time is expressed in terms of pulse widths. Indefinite stability thus corresponds to a zero value of this measure.

Figures 4-6 show results for cubes, spheres and the almond, with the timestep quoted in terms of a fraction of a transit time. We see quite consistent behaviour between the cases. The solution is seen to be least stable with short timesteps in all cases. However, even for the shortest timesteps we have used, it is noteworthy that the analysis is stable for ~3 to 50 pulse widths, or ~8 to 20 transit times for the present bodies; longer than most analyses would be in practice pursued. As the timestep is increased the behaviour is characterised by stability being the norm, with occasional, isolated timestep values giving rise to instability. Note that in this context we are describing stability for say ~20 pulse widths (many tens of transits here) as 'instability'.

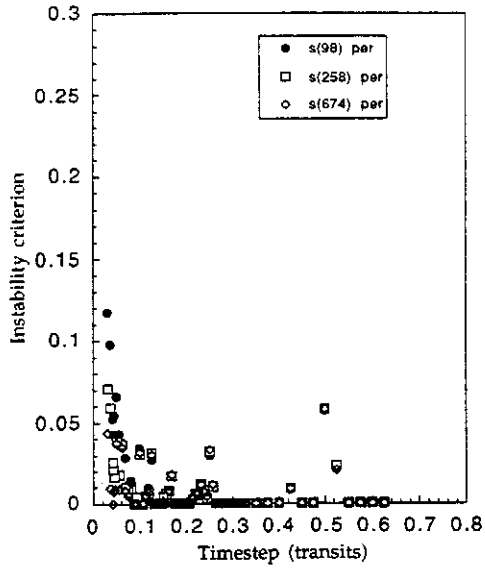

Figure 5. Instability criterion versus timestep in transits for various sphere meshes.

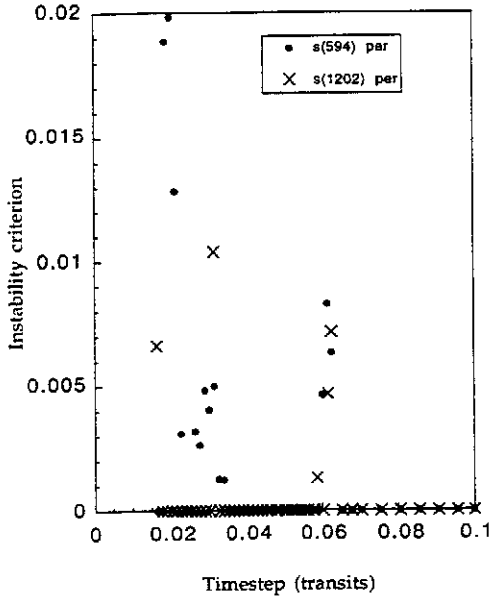

Figure 6. Instability criterion versus timestep, for various almond meshes. Timestep measured in transit times.

One noteworthy characteristic is that these large-timestep instabilities seem to occur in clusters; at a given (group of) timestep(s), independent of the mesh. An example is for timesteps in the range 0.46 to 0.52 for the cube (figure 4). All of these representations are simultaneously 'unstable' (albeit after ~70 to 300 transits of the cube), although the linear spatial discretisation differs by an order of magnitude. Note that the periods of the nearest internal resonances of the cube, at ~0.38 and ~0.58, are outside this range of unstable timesteps. Similar behaviour is observed at a timestep of 0.06 for the almond.

4.2.3 Practical stability criterion

Our principal objective here is to identify practical modelling rules which will provide stability, within the constraints of proper spatial and temporal representation of the field, and the overarching need to minimise computational cost.

the full data from figures 4-6 would extend to ~8 to 10 by this measure.) The association of instability with increasing tendency towards explicitness is clear, although as mentioned above, even the worst cases are stable for many transit times or pulse durations. Note that none of these cases are literally explicit; this requires a very artificial and inaccurate combination of tiny timestep and very coarse quadrature (as does any explicit approach). However, the grave stability difficulties to be expected from an explicit treatment are clear.

Spatial variation of field will (at least in the direction of propagation) be on a length scale of at most the wavelength, and it could be more rapid if the geometry is complex. The temporal 'length scale' is naturally always the period, making the maximum rational timestep equal to the largest nodal separation for a rationally meshed body. A larger value implies loss in accuracy, or equivalently wasted effort occasioned by excessively fine spatial discretisation.

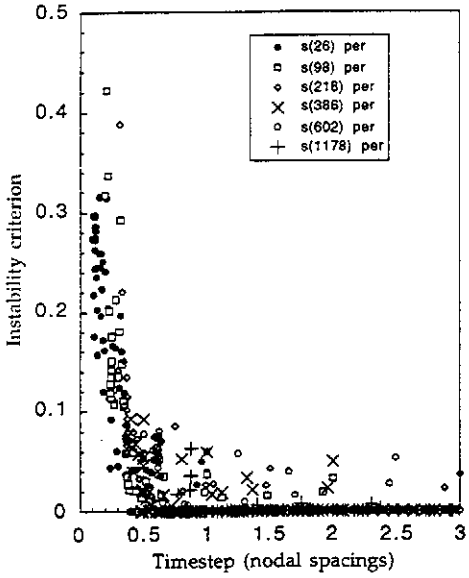

Figure 7. Instability criterion versus timestep, for various cube meshes. Timestep in nodal separations.

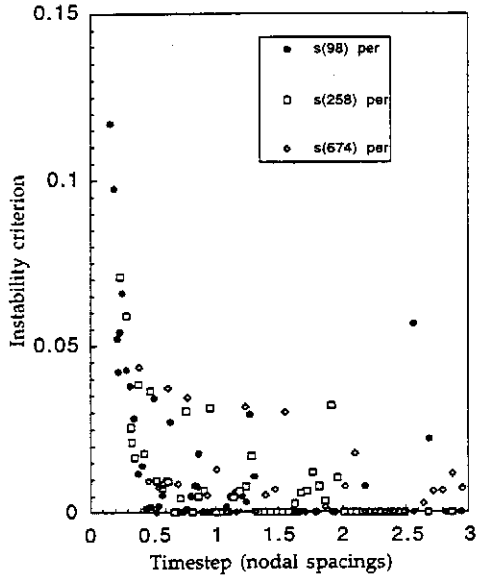

Figure 8. Instability criterion versus timestep, for various sphere meshes. Timestep in nodal separations.

Figures 7, 8 and 9 show results with the timesteps normalised by maximum (element edge) nodal spacings. (Note that only timesteps up to 3 are shown;

Examination of figures 7 to 9 shows that selection of such a timestep for all practical purposes guarantees

stability. The ~20 pulse widths till the field begins to rise on even the cube is here many tens of transit times; more than an order of magnitude more than is generally necessary. Whilst hardly a 'real' scatterer, the almond is less artificially uniform and symmetric than the cube or sphere. The behaviour it exhibits is in our experience typical of more complex bodies (and note the y axis scale of figure 9 differs from figures 7 and 8). Such 'instabilities' as do exist come to light after O(100) or more pulse widths. To put this in perspective, 100 pulse widths corresponds roughly to 4 transits of a 10 wavelength long body. Even these instabilities occur at isolated timestep values, surrounded by stable ones. Should it ever become necessary, a small change in timestep avoids any unfortunate initial selection. No figure is shown here, but as an example typical of many, one of the larger almonds we have analysed comprised 4154 nodes[12], with pulsed illumination to permit analysis as a 8 1/2 wavelength body. No instability was observed for the 3 transits of the run, by when field magnitudes were ~1/100 of the magnitude of the incident pulse.

We close with an example of a more realistic geometry, of the penetration of a pulse into a cavity. The geometry and mesh is shown inset in figure 10. The unit magnitude plane gauss pulse, of half width ~1/2 of the cavity length, is incident normally on the partly open end. The mesh comprises 1517 nodes, and the timestep is roughly equal to the maximum nodal separation, and 1/10 of the pulse half width. The figure shows the surface current density, in the polarisation direction, at two locations on-axis; inside and outside the rear face. On the outside the incident wave is apparent, followed by a very low amplitude roughly harmonic oscillation as energy escapes from the cavity. On the inside the initial pulse is naturally more muted, but the subsequent periodic 'ringing', with a steadily diminishing amplitude, is clear. For present purposes the stability is of most interest; the response is clearly stable for the ~30 transit times for which the analysis was continued.

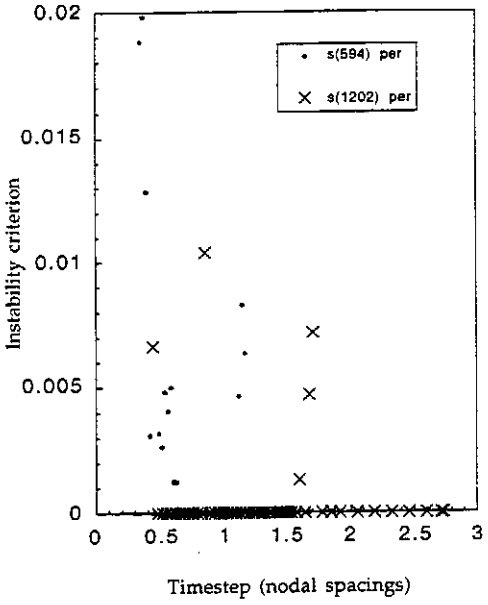

Figure 9. Instability criterion versus timestep, for various almond meshes. Timestep measured in nodal separations.

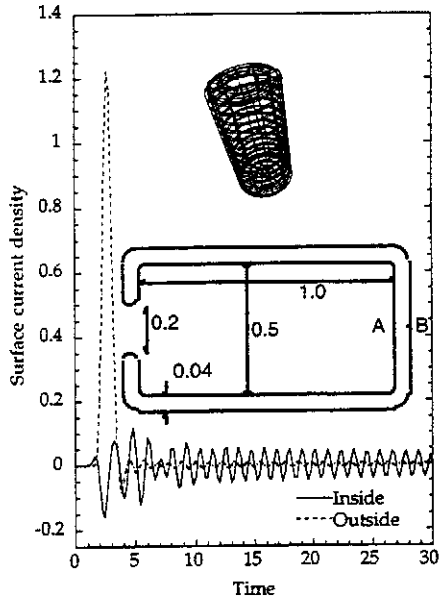

Figure 10 Surface current due to a Gaussian pulse incident on the cavity. On axis, inside and outside rear face. Pulse width ~1/2 cavity length, duration of analysis ~30 transits. Inset: cavity geometry, and 1 517 node mesh of the cavity.

5. DISCUSSION AND CONCLUSIONS

Regardless of stability, implicit approaches are more or less essential for large practical scattering analyses. The alternative explicit approach constrains the timestep to follow the smallest nodal separation. For most real problems there are parts of the geometry which require a fine mesh, and the net effect is a significant multiple in computational cost.

The instability reported for time domain integral equation treatments has been shown here to be essentially a feature of this explicitness. With implicit methods there is no need to employ the averaging schemes, with associated loss of accuracy and cost increase, which have been extensively reported and applied to stabilise explicit treatments. When the larger timesteps which implicitness allows are used stability ceases to be a practical problem. The rational choice of timestep is about the same as a nodal separation. It has been demonstrated that implicit formulations, adopting such a timestep, are for practical purposes immune from instability.

As the references cited show, with the stability issue eliminated, the IETD is able to tackle sizeable scattering problems, providing a useful complement to integral equation frequency domain and FDTD approaches.

Acknowledgements

The support of various sponsors, including British Aerospace, the Ministry of Defence, the Engineering and Physical Sciences Research Council and the Medical Research Council is gratefully acknowledged.

References

1. E. K. Miller, Time-domain modelling in electromagnetics, *Journal of Electromagnetic Waves and Applications*, 8, pp. 1125-1172, 1978.

2. E. K. Miller, A selective survey of computational electromagnetics, *IEEE Transactions on Antennas and Propagation*, 36, pp. 1281-1305, 1988.

3. A. Taflove, *Computational Electromagnetics; The Finite Difference Time Domain Method*. Boston: Artech House, 1995.

4. B. P. Rynne, Stability and convergence of time marching methods in scattering problems, *IMA Journal of Applied Math.* 35, pp. 297-310, 1985.

5. B. P. Rynne, Instabilities in time marching methods for scattering problems, *Electromagnetics*, 6, pp. 129-144, 1986.

6. P. D. Smith, Instabilities in time marching methods for scattering; cause and rectification, *Electromagnetics*, 10, pp. 439-451, 1990.

7. S. M. Rao and D. R. Wilton, Transient scattering by conducting surfaces of arbitrary shape, *IEEE Trans on Antennas and Propagation*, 39, pp. 56-61, 1991.

8. D. A. Vechinski and S. M. Rao, A stable procedure to calculate the transient scattering by conducting surfaces of arbitrary shape, *IEEE Transactions on Antennas and Propagation*, 40, pp. 661-665, 1992.

9. D. A. Vechinski, S. M. Rao, and T. K. Sarkar, Transient scattering from three-dimensional arbitrary shaped dielectric bodies, *J.Opt.Soc.Am.*, 11, pp. 1458-1470, 1994.

10. M. J. Bluck, Integral Equation Methods for Transient Wave Propagation, PhD thesis, Mechanical Engineering Department, Imperial College, University of London, 1993.

11. M. J. Bluck and S. P. Walker, Time Domain BIE Analysis of Large Three Dimensional Electromagnetic Scattering Problems, *IEEE Transactions on Antennas and Propagation*, 45, pp. 894-901, 1997.

12. S. P. Walker, M. J. Bluck, M. D. Pocock, C. Y. Leung, and S. J. Dodson, Curvilinear, isoparametric modelling for rcs prediction, using time domain integral equations, 12th Ann Rev of Progress in Applied Computational Electromagnetics, Monterey CA, vol. 1, pp. 196-204, ACES, 1996.

13. L. B. Gravelle and J. P. Estienne, A numerically stable method of moments time domain model, *12th Annual Rev Prog Appl Comp.Electromagnetics*, , pp. 1238-1247, 1996.

14. M. J. Bluck and S. P. Walker, Analysis of three dimensional transient acoustic wave propagation using the boundary integral equation method, *International Journal for Numerical Methods in Engineering*, 39, pp. 1419-1431, 1996.

15. M. J. Bluck, M. D. Pocock, and S. P. Walker, An accurate method for the calculation of singular integrals arising in time-domain integral equation analysis of electromagnetic scattering, *IEEE Tr on Antennas and Propagation*, 45, pp. 1793-1798, 1997.

16. S. P. Walker and C. Y. Leung, Parallel computation of time domain integral equation analyses of electromagnetic scattering and rcs, *IEEE Transactions on Antennas and Propagation*, 45, pp. 614-619, 1997.

17. S. J. Dodson, S. P. Walker, and M. J. Bluck, Optimisation and large scale computation in integral equation scattering analyses, *ACES Journal*, 13, pp. 131-146, 1998.

18. S. J. Dodson, S. P. Walker, and M. J. Bluck, Costs and cost scalings in time domain integral equation analysis of electromagnetic scattering, *IEEE Antennas and Propagation Magazine* (in press), 1998

19. A. C. Woo, H. T. G. Wang, and M. J. Schuh, Benchmark radar targets for the validation of computational electromagnetics programs, *IEEE Antennas and Propagation Magazine*, 35, pp. 84-89, 1993.